DISTRIBUTION OF THE HEAT AND MASS TRANSFER PARAMETERS WITH A REACTION FRONT WITHIN A LAMINAR BOUNDARY LAYER

A. V. Lykov and G. T. Sergeev

UDC 532.517:536.46

The distribution of Prandtl numbers, Schmidt numbers, Lewis numbers, temperature, enthalpy, concentration, shearing stresses, diffusion currents, and thermal fluxes across the height of a boundary layer within which there exists a reaction front is established and analyzed.

An analytical study is made here of heat and mass transfer in a reacting boundary layer at a porous graphite plate, with injection of a reactant (hydrogen) taken into account. In an earlier study [1] the injected gas was assumed to react with the solid material at the plate surface, as would be the case at a low injection rate, but in this study we will be concerned with both external and internal heat and mass transfer when the injected gas may filter through the porous graphite plate into the laminar boundary layer of a multicomponent gas at a higher rate. The problem has already been formulated in [2]. The analysis here will be based on the assumption that the homogeneous reaction between the injected gas (hydrogen) and the oxygen from the outer stream

$$H_2 + \frac{1}{2}O_2 = H_2O \qquad (a)$$

occurs within an infinitesimally thin zone $y = y_*$ which happens to be the separation surface; that the heterogeneous reaction between the generated water vapor and the carbon of the plate

$$H_2O + C = CO + H_2 \qquad (b)$$

and the homogeneous reaction between the generated carbon monoxide and the oxygen

$$CO + \frac{1}{2}O_2 = CO_2, \qquad (c)$$

are both infinitely faster, as is reaction (a), than the diffusion process and that they occur at the plate surface and within zone $y = y_*$ respectively; that the rate V at which the plate surface shifts as a result of reaction (b) is a function of the x-coordinate only and does not vary with time:

$$V = \frac{\rho_\infty}{2\rho_{\Sigma_e}}\left(\frac{\nu_\infty u_\infty}{x}\right)^{1/2} A, \quad A < 0,$$

while the transverse flow of gases at the plate surface is determined according to the relation

$$(\rho v)_{tg}^{-} = \frac{\rho_\infty}{2}\left(\frac{\nu_\infty u_\infty}{x}\right)^{1/2} B,$$

where A and B are dimensionless constants. All other assumptions have already been stated in [2].

According to the stipulated process pattern, this system contains the gases O_2, CO, H_2O, N_2H_2, and CO_2, which will be denoted by the subscripts 1, 2, 3, 4, 5, 6 respectively: components 2, 3, 4, 5, 6 in the region $0 \le y \le y_*$ (zone I) between the plate surface and the reaction front, components 1, 3, 4, 6 in the region $y > y_*$ (zone II), inside the porous graphite plate components 2, 4, 5, 6.

The system of equations for a laminar layer of a compressible gas, with internal and external heat

Institute of Heat and Mass Transfer, Academy of Sciences of the BSSR, Minsk. Translated from Inzhenerno-Fizicheskii Zhurnal, Vol. 26, No. 5, pp. 807-819, May, 1974. Original article submitted April 26, 1973.

and mass transfer taken into account [2] (here and henceforth a prime sign denotes the derivative with respect to $\tilde{u} = u/u_\infty$):†

$$2\omega\omega'' + \tilde{\rho}\tilde{\mu}\tilde{u} = 0,\ (\omega\bar{j}_i)' + \omega' Y_i' = 0,\ i_{\rm I} = 2,\ 3,\ 4,\ 5,\ 6,\ i_{\rm II} = 1,\ 2,\ 3,\ 6,$$

$$\left\{\omega\left[-\frac{H'}{\rm Pr} - \left(1 - \frac{1}{\rm Pr}\right)u_\infty^2\tilde{u} + \sum_i h_i\left(\frac{Y_i}{\rm Pr} + \bar{j}_i\right)\right]\right\}' + \omega' H' = 0, \tag{1}$$

$$i_{\rm I} = 2,\ 3,\ 4,\ 5,\ 6,\quad i_{\rm II} = 1,\ 3,\ 4,\ 6,$$

with the following boundary conditions:

$$\omega(1) = 0;\ Y_1(1) = Y_{1\infty};\ Y_3(1) = Y_6(1) = 0;\ H(1) = H_\infty \quad \text{at} \quad \tilde{u} = 1;$$

$$Y_i(\tilde{u}_*) = Y_{i*},\ i = 3,\ 6;\ Y_1(\tilde{u}_*) = Y_5(\tilde{u}_*) = Y_2(\tilde{u}_*) = 0; \tag{2}$$

$$\bar{j}_5^{\rm I} = r_{\rm IV}(\bar{j}_3^{\rm II} - \bar{j}_3^{\rm I}),\quad r_{\rm II}\bar{j}_2^{\rm I} = r_{\rm I}(\bar{j}_6^{\rm I} - \bar{j}_6^{\rm II}),\quad \bar{j}_1^{\rm II} = r_{\rm III}(\bar{j}_3^{\rm I} - \bar{j}_3^{\rm II})$$

$$+ r_{\rm V}(\bar{j}_6^{\rm I} - \bar{j}_6^{\rm II});\quad H(\tilde{u}_*) = H_*;$$

$$(\lambda T')^{\rm I} - (\lambda T')^{\rm II} = -\mu_*(Q_{R2}\bar{j}_2^{\rm I} + Q_{R5}\bar{j}_5^{\rm I}) \quad \text{at} \quad \tilde{u} = \tilde{u}_*;$$

$$\omega'(0) = B^*/2;\quad Y_i(0) = Y_{i\rm p},\ i = 2,\ 5,\ 6;\ Y_3(0) = 0;\ H(0) = H_{\rm p}; \tag{3}$$

$$r_{\rm VI}\Omega_2 + r_{\rm III}\Omega_3 + r_{\rm V}\Omega_6 + \omega'(0)Y_{\rm s}s_1 = 0;$$

$$r_{\rm IV}\Omega_3 + \Omega_5 + \omega'(0)Y_{\rm s}s_5 = 0;$$

$$r_{\rm I}\Omega_2 + r_{\rm II}\Omega_6 + \omega'(0)Y_{\rm s}s_{\rm s} - \bar{J}_{\rm s}/2 = 0,\quad \bar{J}_{\rm s} = 2r\omega(0)\bar{j}_3^+;$$

$$-\bar{J}_{\rm c}Q_{\rm Rc} = [2\omega(0)/{\rm Pr}(0)]\left[H' - \sum_i h_i Y_i'\right] - AT_e c_{P\Sigma e}[\Delta M_{i\rm g}(0)$$

$$+ \Delta n_{i\rm g}(0)],\quad i = 2,\ 3,\ 4,\ 5,\ 6,\quad i_{\rm g} = 2,\ 4,\ 5,\ 6 \quad \text{at} \quad \tilde{u} = 0.$$

Here

$$\Omega_i = \Omega_i(0) = \bar{j}_i^+\omega(0) + \xi P\Delta {\rm D}_{\rm i}(0),$$

$$\bar{J}_{\rm s} = (1 - P)K_{\rm s}A,\quad Y_{\rm s} = (1 - P)K_{\rm s},\quad B^* = B + K_\Sigma A,$$

$$\Delta n_i(0) = n_i(1,\ Y_{ie}) - n_i(k,\ Y_{i\rm p}),\quad \Delta M i(0) = M(1,\ Y_{ie}) - M(k,\ Y_{i\rm n}),$$

$$s_1 = Y_1 + r_{\rm VI}Y_2 + r_{\rm V}Y_6,\quad s_5 = r_{\rm IV}Y_3 + Y_5,\quad s_{\rm s} = r_{\rm II}Y_2 + r_{\rm I}Y_6,$$

$$Q_{R\rm s} = h_{\rm s} + r^{-1}h_3 - r_{\rm II}^{-1}h_2 - r_{\rm VII}h_5,$$

$$Q_{R2} = h_2 + r_{\rm VI}h_1 - r_{\rm V}^{-1}h_6,\quad Q_{R5} = h_5 + r_{\rm VIII}h_1 - r_{\rm IV}^{-1}h_3,$$

where

$$r = \bar{m}_{\rm c}/\bar{m}_3;\quad r_{\rm VII} = \bar{m}_5/\bar{m}_{\rm c};\quad r_{\rm VIII} = \bar{m}_1/2\bar{m}_5;\quad k = T_{\Sigma\rm p}/T_e;$$

$$n_i = (\lambda_{\Sigma e}T_e)^{-1}\sum_{i_{\rm r}}\int \Gamma dY_{i\rm g};\quad M_i = \int F d\theta,\ {\rm D}_{\rm i} = \int \Gamma dY_{i\rm g};$$

$$\xi = A/2\gamma\rho_{\Sigma e};\quad K_{\rm s} = \rho_{\rm c}/\rho_\Sigma;\quad K_\Sigma = \rho_{\Sigma\rm p}/\rho_{\Sigma e};\quad \bar{j}_i = -Y_i'/{\rm Sc}_i.$$

In order to close the system (1)-(4), it is necessary to supplement it with the equation of state

$$P = R\rho T\sum_i Y_i/\bar{m}_i,\ i_{\rm I} = 2,\ 3,\ 4,\ 5 \text{ and } 6,$$

$$i_{\rm II} = 1,\ 2,\ 3,\ 4 \text{ and } 6,\ i_{\rm r} = 2,\ 4,\ 5 \text{ and } 6, \tag{5}$$

and the synthesis of binary diffusion

$$\frac{\mu}{\rho}\sum_{K=1}^{N=6}\frac{Y_K}{\bar{m}_K D_{iK}}\left(\frac{\bar{j}_i}{Y_i} - \frac{\bar{j}_K}{Y_K}\right) = \sum_{K=1}^{N=6}\frac{Y_K}{\bar{m}_K}\left(\frac{Y_K'}{Y_K} - \frac{Y_i'}{Y_i}\right),\ K \neq i, \tag{6}$$

as well as with the formulas for the thermophysical parameter $F_{\rm i}$ (i referring to the component gases) and F (referring to the gas mixture)

$$F_i = F_i(\bar{m}_i,\ \sigma_i,\ T),\quad F = F(Y_i,\ F_i), \tag{7}$$

where $F_{\rm i}$ or F denote the density (weight), the viscosity, the thermal conductivity, the specific heat, the thermal diffusivity, or the diffusivity (binary and overall). The respective formulas are given in [4].

†Other symbols have the same meaning as in [2].

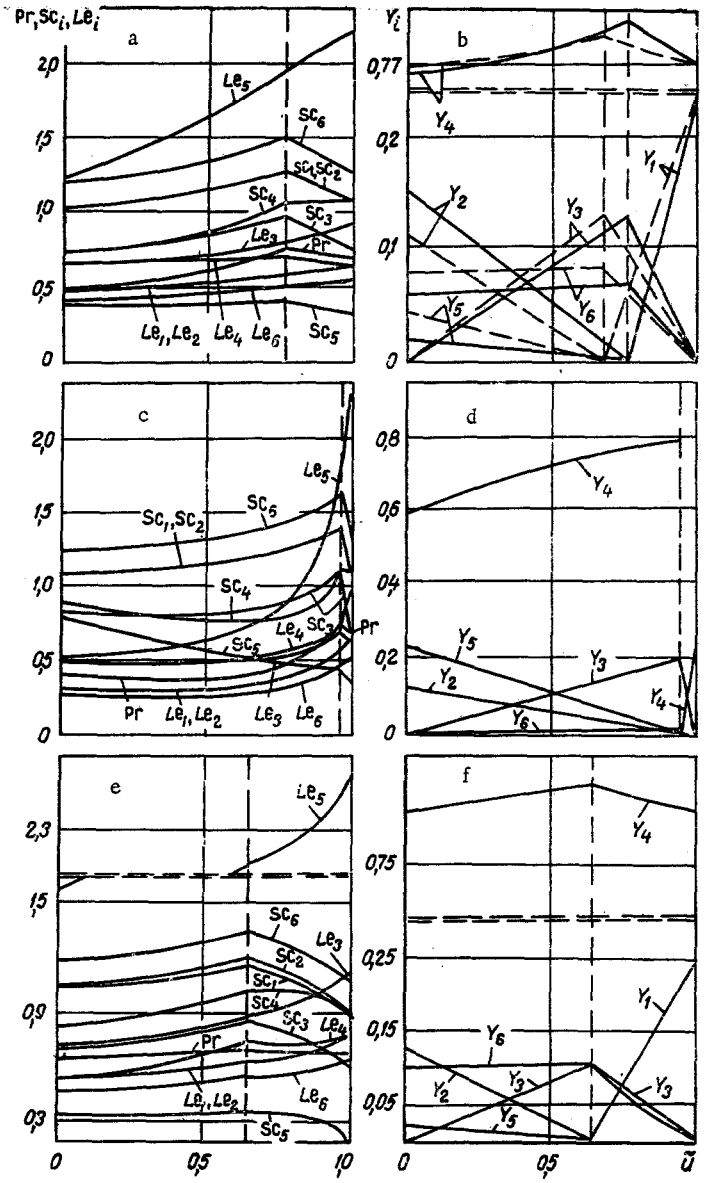

Fig. 1. Variation of Pr, Sc_i, Le_i, Y_i, and $\bar{j}_i$ across the height of a boundary layer $\tilde{u}$: a) and b) $T_\infty = 1800°K$, $u_\infty = 15$ m/sec, P = 0.2, B = 0.067; c) and d) T = 1800°K, $u_\infty = 15$ m/sec, P = 0.2, B = 0.27; e) and f) $T_\infty = 600°K$, $u_\infty = 15$ m/sec, P = 0.2, B = 0.067; in b) solid line refers to $Pr \neq Sc_i \neq 1$, dashed line refers to $Pr = Sc_i = \tilde{\mu}\tilde{\rho} = 1$.

The nonlinear system (1)-(7), which contains not only the sought functions but also the unknowns

$$A,\ \tilde{u}_*,\ H_*\ (\text{or } T_*),\ H_p\ (\text{or } T_p),\ Y_{i*},\ i = 3,\ 6 \quad \text{and} \quad Y_i(0),\ i = 2,\ 5,\ 6,$$

was integrated numerically by the iteration method. Approximate values were assigned to the unknown quantities first, then the momentum equation, the constant-total-concentration equation, and the constant-total-enthalpy equation were solved successively, whereupon the coefficients F_i and F were determined. This computation cycle was repeated until resulting values of the temperature did not differ from the values obtained in the preceding cycle by more than an a priori specified number of degrees. The momentum equation was then solved in a similar manner and checked for the conditions at the reaction front. If these conditions had not been satisfied, then a new location of this front was assumed and other approximate values were stipulated for the concentration and the enthalpy. The computation cycle was then

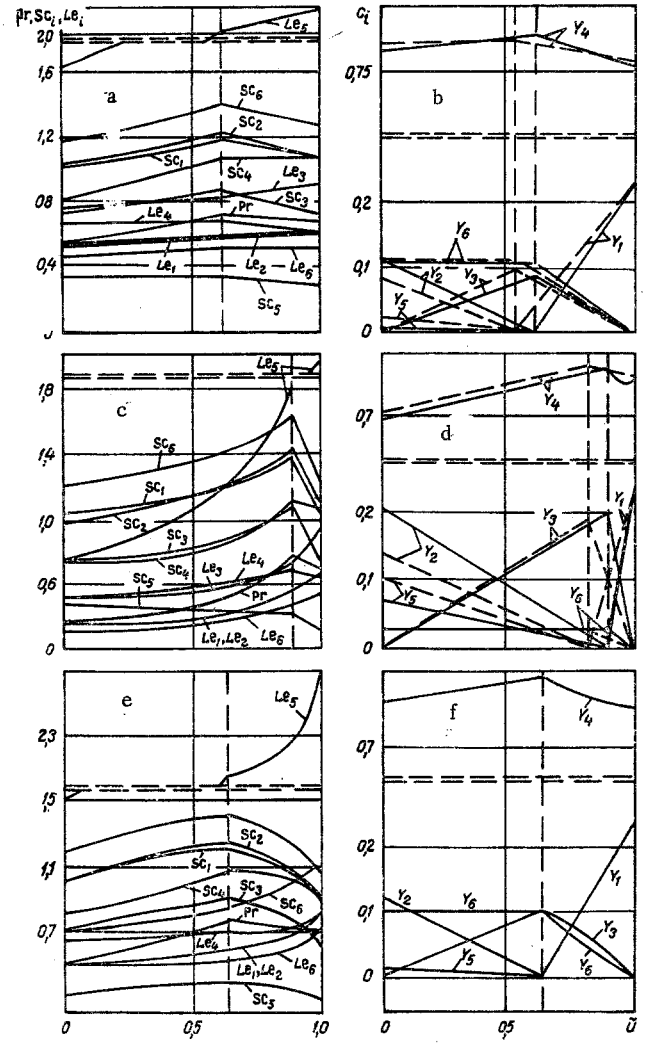

Fig. 2. Pr, Sc_i, Le_i, Y_i, and $\bar{j}_i$ as functions of $\tilde{u}$, at following values of the boundary-layer parameters: a) and b) T_∞ = 1800°K, u_∞ = 15 m/sec, P = 0.2, B = 0.067; c) and d) T_∞ = 1800°K, u_∞ = 15 m/sec, B = 0.27; e) and f) T_∞ = 600°K, u_∞ = 100 m/sec, P = 0.2, B = 0.067; in b) and d) solid line refers to Pr ≠ Sc_i ≠ 1, dashed line refers to Pr = Sc_i = $\tilde{\mu}\tilde{\rho}$ = 1.

repeated until those conditions had become satisfied and the problem could thus be regarded as having been solved. This numerical integration was performed on a model MINSK-22 computer.

The results of this numerical calculation are shown in Figs. 1-4 and in Tables 1-2, along with data on the solution to problem (1)-(7) for Pr = Sc_i = 1 and $\tilde{\mu}\tilde{\rho}$ = const. In this latter case both the enthalpy and the concentration are distributed linearly:

$$H^{\mathrm{I}} = H_p + (H_* - H_p)\,\tilde{u}/\tilde{u}_*, \quad H^{\mathrm{II}} = H_* + (H_\infty - H_*)\,(\tilde{u} - \tilde{u}_*)/(1 - \tilde{u}_*),$$
$$Y_i^{\mathrm{I}} = Y_{ip} + (Y_{i*} - Y_{ip})\,\tilde{u}/\tilde{u}_*, \quad Y_i^{\mathrm{II}} = Y_{i*} + (Y_{i\infty} - Y_{i*})\,(\tilde{u} - \tilde{u}_*)/(1 - \tilde{u}_*), \qquad (8)$$
$$i_{\mathrm{I}} = 2,\ 3,\ 5,\ 6, \quad i_{\mathrm{II}} = 1,\ 2,\ 3,\ 6.$$

The velocity distribution $\omega(\tilde{u})$ is found, according to [3],

$$\omega(\tilde{u}) = u_0^{-3/2}\omega_\gamma(\tilde{u}u_0), \qquad (9)$$

where $\tilde{u}_0$ are the zeroes of function ω_γ. The unknowns H_p, H_*, $\tilde{u}_*$, Y_{ip}, and Y_{i*} are found from condition (2), where $B^*/2 = u_0^{-1/2}\mathrm{tg}\gamma$ and $\gamma = \mathrm{arc\,tg}\,\omega_\gamma(0)$. From the last condition in (3) and taking into account (8), we obtain the following relation for locating the reaction front $\tilde{u}_*$ when Pr = Sc_i = 1 and $\tilde{\mu}\tilde{\rho}$ = const:

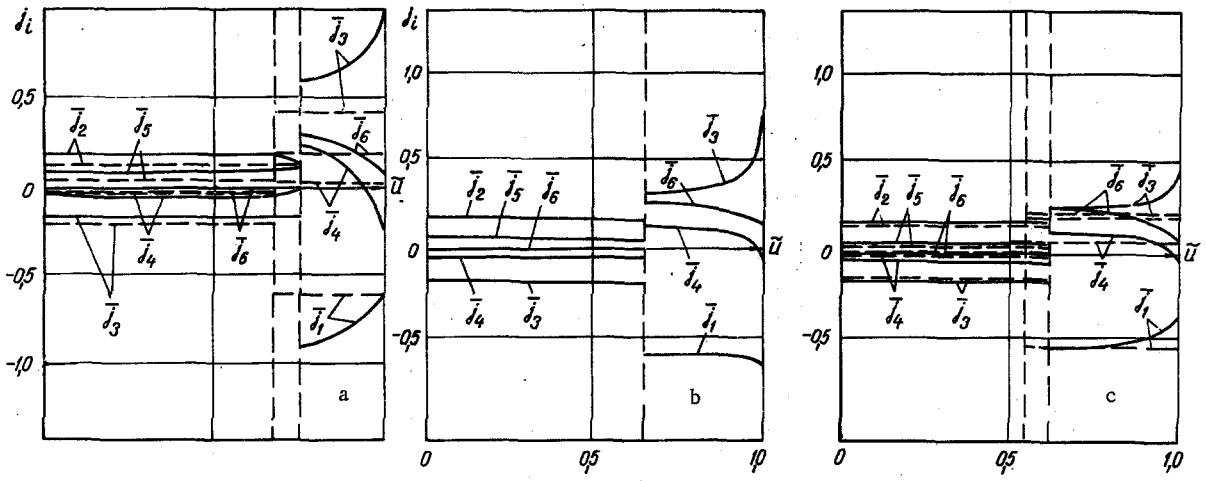

Fig. 3. Variation of normalized currents $\bar{j}_i$ across the height of a boundary layer $\tilde{u}$, at $u_\infty = 15$ m/sec and B = 0.067: a) $T_\infty = 1800°K$, B = 0.067, P = 0.4; b) $T_\infty = 600°K$, B = 0.067, P = 0.2; c) $T_\infty = 1800°K$, B = 0.067, P = 0.2; in a) solid line refers to $Pr \neq Sc_i \neq 1$, dashed line refers to Pr = $Sc_i = \tilde{\mu}\tilde{\rho} = 1$.

$$(\Phi u_\infty^2/2)\tilde{u}_*^2 + \tilde{u}_*\left[H_p - \sum_{i_I} h_{i*}Y_{ip} - H_\infty + h_{1*}Y_{1\infty} + h_{4*}Y_{4\infty} + Q_{R5}Y_{5p} + Q_{R2}Y_{2p}\right] + \sum_{i_I} h_{i*}Y_{ip} - (Q_{R5}Y_{5p} + Q_{R2}Y_{2p}) - H_p = 0, \quad (10)$$

$$i_I = 2,\ 4,\ 5,\ 6.$$

Here $H_p = \sum_{i_I} h_i Y_{ip}$; i = 2, 4, 5, 6; $\Phi = (gI)^{-1}$; g denotes the acceleration due to gravity, and I denotes the mechanical equivalent of heat.

When solving the quadratic equation (10), one must select the root $\tilde{u}_*$ so that $0 < \tilde{u}_* < 1$. With the viscous dissipation disregarded, $(\Phi u_\infty^2) \to 0$ and (10) transforms into a first-order equation with respect to u_*.

Taking into account relation (9), we find the friction coefficient at the surface

$$c_f = 2\omega_p/\sqrt{Re_x} \quad (11)$$

and the thermal flux

$$q_p = -\left[\left(\lambda\frac{\omega}{\mu}\right)_p \frac{\rho_\infty u_\infty}{\sqrt{Re_x}}\right] T_p'; \quad (12)$$

for the general case; when Pr = $Sc_i = \tilde{\mu}\tilde{\rho} = 1$, then function $\omega_p = \omega(0) = u_0^{-3/2}$.

It follows from the solution to problem (1)-(7), as shown in the general form in Figs. 1-3, that the Prandtl number Pr, the Schmidt numbers Sc_i, and the Lewis numbers Le_i, as well as the normalized diffusion currents $\bar{j}_i$ change very much within the region $\tilde{u} > 0.5$, especially near the reaction zone $\tilde{u} = \tilde{u}_*$ (indicated in Figs. 1-3 by the dashed vertical straight line). The most significant changes in $\bar{j}_i$ occur within the region $\tilde{u} \to 1$, i.e., at the outer edge of the boundary layer. Where $\tilde{u} < 0.5$ the changes in Pr, Sc_i, Le_i, and $\bar{j}_i$ are negligible, while the concentrations $Y_i = Y_i(\tilde{u})$ become almost linearly distributed within zones I and II. The absolute values of Y_i and $\bar{j}_i$, as well as the location of the reaction front $\tilde{u}_*$ (Figs. 1, 2), become quite different when $Pr \neq Sc_i \neq 1$ and when $Pr = Sc_i = 1$. This difference is most distinct in the case of $Y_i(0)$, i = 2, 5. Thus, for $Pr = Sc_i = 1$ we have $Y_2(0) = 0.160$ and $Y_5(0) = 0.111$, while for $Pr \neq Sc_i \neq 1$ we have $Y_2(0) = 0.210$ and $Y_5 = 0.074$ (Fig. 2d). The values of $\tilde{u}_*$ differ by approximately 13%. While the Prandtl number remains almost constant across the height of the boundary layer when the injection rate is low (small B-number) (Fig. 1e, B = 0.067), it changes appreciably at high injection rates (Figs. 1c and 2c, B = 0.27). As the rate of hydrogen injection increases, moreover, the reaction front $\tilde{u}_*$ shifts (is "displaced") toward the outer edge of the boundary reaction front ($\tilde{u}_* = 0.77$ at B = 0.067 and $\tilde{u}_* = 0.97$ at B = 0.27, Fig. 1a, c). Meanwhile, $Sc_5(0)$ decreases appreciably and so does $Le_5(0)$ accordingly (Figs. 1a, c

and 2a, c). The other numbers Sc_i and Le_i do not change as much with a change in the injection rate (B-number). Pr(0) decreases somewhat with a higher B-number, because the concentration $Y_5(0)$ becomes higher and the Prandtl number for hydrogen is smaller than the respective Prandtl number for all other components of the gas mixture. Furthermore, an increase in the B-number causes an increase in Y_3 and $\bar{j}_3$, because the injected gas (hydrogen H_2) is completely converted to water (H_2O) according to reaction (a) (Figs. 1b, d, 2d, and 3). An increase in concentration $Y_3(\tilde{u}_*)$ produces an increase in Y_2 and $\bar{j}_2$ (reaction (b)) and, consequently, also an increase in Y_6 and $\bar{j}_6$ (reaction (c)). Meanwhile, Y_4 and $\bar{j}_4$ change very little, because nitrogen (N_2) is in this case an inert gas. The concentration $Y_1(\tilde{u})$ and the normalized current $\bar{j}_1(\tilde{u})$ remain unchanged during a change in the injection rate B (Fig. 1-3), because the entire oxygen (at a given constant concentration $Y_{1\infty}$) is used up stoichiometrically according to reactions (a) and (c).

It follows from Figs. 1 and 2 that the Prandtl number varies across the height of a boundary layer, quite appreciably sometimes. Thus, at $T_\infty = 600°K$, $B = 0.067$, $P = 0.2$, and $u_\infty = 15$ m/sec (fifth variant) we have $Pr = 0.525$, 0.718, and 0.683 respectively when $\tilde{u} = 0$, $\tilde{u} = \tilde{u}_* = 0.64$, and $\tilde{u} = 1$; at $T_\infty = 1800°K$, $B = 0.27$, $P = 0.2$, and $u_\infty = 15$ m/sec (fourth variant) we have $Pr|_{\tilde{u}=0} = 0.387$, $Pr|_{\tilde{u}=\tilde{u}_*=0.97} = 0.781$, and $Pr|_{\tilde{u}=1} = 0.689$.

The largest variations across the height of a boundary layer occur in Lewis numbers and in Schmidt numbers, especially in Le_5. Thus, while $Le_5 = 0.501$ at $\tilde{u} = 0$, we have $Le_5 = 1.844$ and 2.168 (variant 2c) at $\tilde{u} = \tilde{u}_* = 0.97$ and $\tilde{u} = 1$ respectively.

At $u_\infty = 15$ m/sec we have $Le_5(0) = 1.561$ and $Le_5(1) = 2.628$ (Fig. 1f), also at $u_\infty = 100$ m/sec we have $Le_5(0) = 1.564$ and $Le_5(1) = 2.628$ (Fig. 2f), i.e., the effect of velocity on $Le_5(\tilde{u})$ and on the other Lewis numbers $Le_i(\tilde{u})$ (i = 1, 2, 3, 4, 6) is weak.

As the molecular weight $\bar{m}_i$ increases, in most cases the Schmidt numbers Sc_i become larger and the Lewis numbers Le_i become smaller, because these numbers depend on the coefficients F_i, F defined in (7) and, consequently, also on the absolute values of $\bar{m}_i$. Since Sc_i and Le_i are functions not only of $\bar{m}_i$ but also of Y_i, however, hence in certain variants this dependence of Sc_i and Le_i on $\bar{m}_i$ ceases to be valid (with the temperature assumed constant) due to the predominant effect of the concentrations Y_i on Sc_i and Le_i (i = 1, 2, 3, 4) (Figs. 1 and 2).

The normalized diffusion currents $\bar{j}_i$ vary most appreciably within the zone $\tilde{u} > \tilde{u}_*$ (Fig. 3). Where $\tilde{u} \leq \tilde{u}_*$, on the other hand, the $\bar{j}_i$ remain almost constant. Within the zone where $\tilde{u} = \tilde{u}_*$ the absolute values of the derivatives Y_i' and, therefore, also of the currents $\bar{j}_i$ have a discontinuity. For comparison, in Fig. 3a are shown the values of $\bar{j}_i$ corresponding to $Pr = Sc_i = 1$ (dashed straight lines). While within the zone where $\tilde{u} \leq \tilde{u}_*$ the absolute values of $\bar{j}_i$ are almost the same, whether the Prandtl number and the Schmidt numbers are constant ($Pr = Sc_i = 1$) or variable, within the zone where $\tilde{u}_* < \tilde{u} \leq 1$ the currents $\bar{j}_i$ differ considerably. A comparison between Fig. 3a and Fig. 3b (respective variants 1 and 6) shows that to a higher porosity P corresponds a higher $\tilde{u}_*$. Thus, $\tilde{u}_* = 0.77$ when $P = 0.4$ (Fig. 3a) and $\tilde{u}_* = 0.61$ when $P = 0.2$ (Fig. 3c), i.e., at higher porosities P and the same injection rate ($B = 0.067$) the total mass flow rate of injected gas per unit plate surface increases, resulting in a shift of the reaction front and thus in a higher $\tilde{u}_*$. As the stream velocity is increased from 15 to 50 m/sec, the parameters ω, ω', H, T, Y_i, Le_i, and $\bar{j}_i$ do not change much. Thus, for $T_\infty = 1800°K$, $B = 0.067$, $P = 0.4$, and $u_\infty = 50$ m/sec we have $\tilde{u}_* = 0.77$, $T_p = 1132°K$, $T_* = 3049°K$, $H_p = -7.7$ J/g, $H_* = 2330$ J/g, $\omega_p = 0.247$, and $\omega_p' = 0.0687$. For $u_\infty = 15$ m/sec and all other conditions unchanged, the values of these parameters, as shown in Figs. 1a-3a and in Table 1, differ from those for $u_\infty = 50$ m/sec by not more than 2%. A comparison between Fig. 3b and Fig. 3c indicates that within zone I the normalized currents $\bar{j}_i$ remain almost the same, but they differ appreciably where $\tilde{u} > \tilde{u}_*$. Thus at $T_\infty = 1800°K$ the ratio $\bar{j}_I^{II}(\tilde{u}_*)/\bar{j}_I^{II}(1)$ is equal to $(-0.559)/(-0.3981)$, $(0.247)/(0.507)$, $(0.108)/(-0.062)$ and $(0.243)/(0.094)$ for i = 1, 3, 4, and 6 respectively (with $\tilde{u}_* = 0.61$) (Fig. 1c). At $T_\infty = 305°K$ and all other parameters unchanged, this ratio is respectively equal to $(-0.655)/(-0.811)$, $(0.352)/(1.012)$, $(0.124)/(-0.109)$, and $(0.248)/(0.188)$ (with $u_* = 0.66$). Furthermore, a higher $\tilde{u}_*$ corresponds to a lower temperature T_∞ (Fig. 3b, c). Or for $B = 0.067$, $P = 0.2$, and $u_\infty = 50$ m/sec, for instance, we have $\tilde{u}_* = 0.63$ at $T_\infty = 1000°K$ and $\tilde{u}_* = 0.617$ at $T_\infty = 1800°K$. It is to be noted that the variation in $\tilde{u}_*$ with temperature T_∞ (within the given range of T_∞ temperatures) is negligible, however, by virtue of the relation $\tilde{u}_* \sim T_\infty^{-1}$, which follows from the last condition in (3) or from Eq. (10).

According to the data in Table 1, a higher injection velocity results in lower T and H at the plate surface, owing to the effect of transpiration cooling; T and H reach their maxima where $\tilde{u} = \tilde{u}_*$, because combustion of the gases according to reactions (a) and (c) occurs within this zone. At the outer edge of the boundary layer H(I) and T(I) are the same at the same stream velocity u_∞.

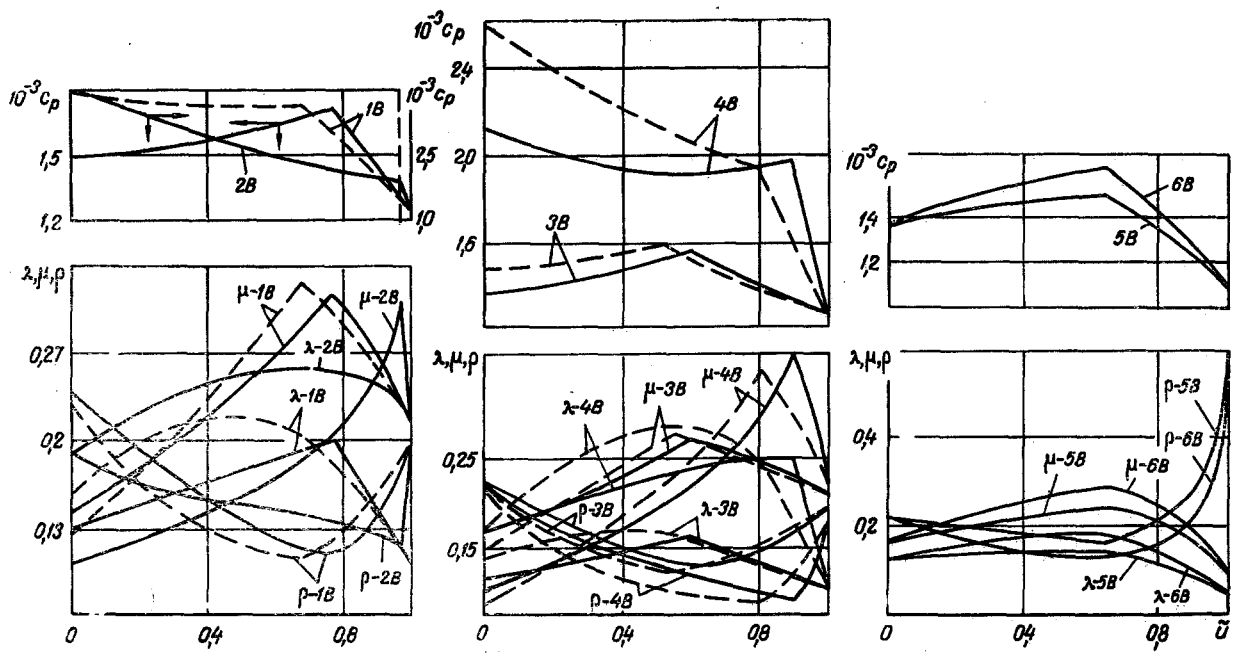

Fig. 4. Specific heat c_p (J/kg·°C), thermal conductivity λ(W/m·°C), dynamic viscosity μ(kg/m·h), and density ρ(kg/m) as functions of $\tilde{u}$; boundary-layer parameters for variants 1_B—6_B are given in Table 1; solid line refers to $Pr \neq Sc_i \neq 1$, dashed line refers to $Pr = Sc_i = \tilde{\mu}\tilde{\rho} = 1$.

At velocities $u_\infty = 15$ and 100 m/sec (variants 5 and 6 in Table 1) the respective values of $H(\tilde{u})$ and $T(\tilde{u})$ are almost the same. Furthermore, a comparison between variants 1_B and 3_B or variants 2_B and 4_B indicates that the $H(\tilde{u})$ field and the $T(\tilde{u})$ field within the zone where $\tilde{u} = \tilde{u}_*$ both depend more on the heat generation than on the porosity. The values of $H(\tilde{u})$ and $T(\tilde{u})$ are higher when $Pr = Sc_i = 1$ than when $Pr \neq Sc_i \neq 1$ (except near the plate surface), inasmuch as in the former case all the chemical energy in the boundary layer is converted to heat. When $Pr \neq Sc_i \neq 1$, then such a conversion is only partial.

The trend of functions $\omega(\tilde{u})$ and $\omega'(\tilde{u})$ is analogous to that shown in [1], inasmuch as the velocity u has no discontinuity at $\tilde{u} = \tilde{u}_*$. In variants 1_B—6_B the values of $\omega(0)$ are respectively 0.248, 0.108, 0.264, 0.1521, 0.216, 0.217, and the values of $\omega'(0)$ are respectively 0.069, 0.1541, 0.066, 0.1630, 0.0615, 0.0614. When $Pr = Sc_i = 1$ and $\tilde{\mu}\tilde{\rho} = 1$, we have for $\omega(0)$ (variants 1_B, 3_B, and 4_B) 0.282, 0.284, 0.215 and for $\omega'(0)$ 0.0694, 0.0666, 0.169. Here, too, $\omega(1) \to 0$ and $\omega'(1) \to \infty$, while both ω and ω' depend more on the injection rate B than on T_p and P within their given ranges. As the injection (hydrogen) rate is increased, the factor $\tilde{\mu}\tilde{\rho}$ in the momentum equation (1) decreases so that, therefore, ω decreases and ω' increases (one may compare $\omega(0)$ and $\omega'(0)$ in variants 1_B and 2_B or in variants 3_B and 4_B, for example). The porosity P affects ω and ω' as does the injection rate B, inasmuch as, at the same injection rate and with the other conditions unchanged, a higher porosity corresponds to a higher total flow rate of injected gas per unit area of the porous surface, which can be demonstrated on the basis of a comparison between $\omega(0)$ and $\omega'(0)$ respectively for variants 1_B and 3_B or variants 2_B and 4_B. A comparison between variants 1_B and 6_B, meanwhile, indicates that ω decreases and ω' increases with rising temperature T_∞.

When $Pr = Sc_i = 1$ and $\tilde{\mu}\tilde{\rho} = 1$, then the ω parameters increase relative to the case of constant Pr and Sc_i, which follows from the particular structure of the first equation in (1), where the condition $Pr = Sc_i = \tilde{\mu}\tilde{\rho} = 1$ corresponds to a higher ω [1]. Maximum ω occurs within the boundary layer. This maximum ω corresponds to $\omega' = \omega'(\tilde{u})$.

The variation of the thermal flux q_p and that of the friction coefficient c_f along the porous plate x, as is shown in Table 2, corresponds to curves $q_p = q_p(x)$ and $c_f = c_f(x)$ in [1], with

$$Q = \frac{1}{l}\int_0^l q_p(x)\,dx \text{ kcal/m}^2\cdot\text{sec},$$

and l denoting the length of the porous plate ($l = 0.5$ m). Here, too, $c_f \to \infty$ and $q_p \to \infty$ at $x = 0$. A comparison between variants 1_B and 2_B or variants 3_B and 4_B indicates that, as the injection rate B increases,

TABLE 1†. Variation of Enthalpy H (J/g) and of Temperature T(°K) across the Height u of a Boundary Layer

$\tilde{u}$	$\Pr \neq Sc_t \neq 1$						$\Pr = Sc_t = 1$		
	^1_B	^2_B	^3_B	^4_B	^5_B	^6_B	^1_B	^3_B	^4_B
				$H \cdot 10$					
0	—13	88	27	1	373	373	146	118	171
0,1	865	1325	946	715	578	576	2061	1770	2324
0,2	2134	2541	2216	1773	828	822	4268	3657	4819
0,3	3554	3389	3602	2868	1149	1139	6475	5544	7314
0,4	5173	4019	5127	4097	1554	1538	8673	7431	9809
0,5	7056	4577	6818	5576	2055	2032	10890	9318	12304
0,6	9223	5232	8714	7414	2670	2639	13097	11130	14799
0,7	12016	6238	11477	10069	3694	3660	15070	12893	17294
0,8	15264	8112	14019	13889	4545	4518	16107	14656	19789
0,9	17487	12381	16108	20128	4728	4712	17144	16418	19159
1,0	17057	17057	17057	17057	3143	3154	18181	18181	18181
				$T \cdot 10$					
0	11430	4631	13930	8014	13863	13817	9615	11993	6998
0,1	13075	5751	15543	9594	14970	14918	12272	14662	9239
0,2	14998	6993	17359	11366	16107	16048	15046	17863	11712
0,3	17039	8314	19240	13283	17298	17233	17943	20094	14452
0,4	19229	9764	21203	15374	18557	18484	20965	22852	17501
0,5	21612	11415	23268	17721	19900	19818	24116	25634	20907
0,6	24252	13382	25465	20448	21352	21261	27400	25810	24728
0,7	27242	15874	24410	23763	20149	20062	29536	24120	29031
0,8	28643	19346	22810	28050	16739	16672	26298	22268	33899
0,9	24713	25119	20916	34192	12611	12568	22494	20234	28043
1,0	18000	18000	18000	18000	6000	6000	18000	18000	18000
$\tilde{u}_*$	0,77	0,97	0,61	0,90	0,64	0,64	0,68	0,54	0,81
$H \cdot 10$	14315	20433	8916	20128	2954	2918	14863	10072	20038
$T_* \cdot 10$	29622	33647	25693	34192	21970	21875	30125	26753	34421

† Subscripts 1_B-6_B denote the following variants under study: 1_B and 2_B B = 0.067 and 0.27 respectively, T_∞ = 1800°K, u_∞ = 15 m/sec, P = 0.2, 3_B and 4_B B = 0.067 and 0.27 respectively, T_∞ = 1800°K, u_∞ = 15 m/sec P = 0.2, 5_B and 6_B u_∞ = 15 and 100 m/sec respectively, T_∞ = 600°K, B = 0.067, P = 0.2

TABLE 2. Variation of Thermal Flux q_p(kcal/m^2 · sec) and of the Friction Coefficient c_f along a Porous Plate (x, cm).

x	$q_p \cdot 10^2$								
	$\Pr \neq Sc_t \neq 1$						$\Pr = Sc_t = 1$		
	^1_B	^2_B	^3_B	^4_B	^5_B	^6_B	^1_B	^3_B	^4_B
1	4188	4111	3350	4371	2210	4010	10732	8083	10850
3	2418	2374	1934	2524	1276	2315	6196	4667	6264
6	1710	1678	1368	1784	902	1637	4381	3300	4429
10	1324	1300	1059	1382	699	1268	3394	2556	3431
15	1081	1062	865	1129	571	1035	2771	2087	2801
20	936	919	749	977	494	897	2400	1807	2426
30	765	751	612	798	403	732	1959	1476	1981
50	592	581	474	618	312	567	1518	1143	1534
$Q \cdot 10^2$	1084	1062	948	1236	624	1124	3036	2286	3068
x	$c_f \cdot 10^4$								
	$\Pr \neq Sc_t \neq 1$						$\Pr = Sc_t = 1$		
	^1_B	^2_B	^3_B	^4_B	^5_B	^6_B	^1_B	^3_B	^4_B
1	224	97	238	137	79	44	255	256	195
3	129	56	137	79	46	25	147	148	113
6	91	40	97	56	32	18	104	105	80
10	71	31	75	43	25	14	80	81	62
15	58	25	61	35	21	11	66	66	50
20	50	22	53	31	18	10	57	57	44
30	41	18	43	25	14	8	46	47	36
50	32	14	34	19	11	6	36	36	28

c_f decreases and q_p changes very little. For the given range of B (a rather narrow range), q_p does not decrease with increasing B, as would be expected, but even tends to slightly increase. An analysis of Eq. (11) shows that, when B increases, the decrease in c_f is due mainly to the decrease in $\omega(0)$, while the

increase in q_p (despite the said variation in $\omega(0)$) is due to the combined effect of several parameters in Eq. (12), which include the temperature gradient T_p'. As the rate of hydrogen injection increases, the endothermal reaction (b) causes a drop in the surface temperature of the plate T_p and an only negligible change in the temperature $T*$; consequently, the derivative T_p' also increases with increasing B. The decrease in c_f and the increase in q_p with increasing u_∞ (Table 2) can also be explained in terms of the relations (11)-(12), where $c_f \sim u_\infty^{-1/2}$ and $q_p \sim u_\infty^{1/2}$. An increase in the porosity of the graphite plate causes a decrease in c_f, by virtue of the decrease in $\omega(0)$ according to (11). Meanwhile, q_p varies little as a function of P. According to the data in Table 2, c_f and q_p have higher values when $Pr = Sc_i = 1$ than when $Pr \neq Sc_i \neq 1$. This is explained by an increase of $\omega(0)$ in (11) ($\omega(0) = u_0^{-3/2}$) for c_f and by an increase also of λ_p and T_p in Table 1 and Fig. 4 for q_p (μ_p is almost the same whether $Pr = Sc_i = \tilde{\mu}\tilde{\rho} = 1$ or $Pr \neq Sc_i \neq 1$). As T_∞ rises (variants 1_B and 5_B in Table 2), q_p and c_f also increase, as a consequence of a higher ω_p and a lower Reynolds number Re_x according to relations (11) and (12); meanwhile, the ratio λ_p/μ_p remains almost constant.

The absolute values of the thermophysical parameters μ, ρ, λ, and $\bar{c}_p$ in Fig. 4 vary appreciably across the height of a boundary layer. The values of these parameters are very different for $Pr = Sc_i = \ldots = 1$ and for $Pr \neq Sc_i \neq 1$ respectively. Thus, for $\mu(0)$, $\mu(\tilde{\mu}_*)$, and $\mu(1)$ we have respectively 0.0624, 0.3602, and 0.2107 (variant 2). Or $\bar{c}_p(0) = 2623.1$ J/kg·°C, $\bar{c}_p(\tilde{u}_*) = 2019.9$ J/kg·°C, $\bar{c}_p(1) = 1246.2$ J/kg·°C, $\tilde{u}* = 0.80$ when $Pr = Sc_i = 1$, for instance, but $\bar{c}_p(0) = 2135.3$ J/kg·°C, $\bar{c}_p(\tilde{u}_*) = 1935.2$ J/kg·°C, $\bar{c}_p(1) = 1246.2$ when $Pr \neq Sc_i \neq 1$ (variant 4_B). The values of ρ and λ across a boundary layer differ by the same order of magnitude.

Thus, the assumption that $Pr = Sc_i = 1$ leads in this case to large departures of calculated thermophysical as well as other heat and mass transfer parameters (c_f, q_p, ω, Y_i, j_i, T, and H) from their respective exact values.

NOTATION

x	is the longitudinal coordinate at the plate surface;
y	is the normal coordinate;
u, v	are the components of the stream velocity along x,y respectively;
R	is the universal gas constant;
p	is the pressure;
c_p	is the specified heat at constant pressure;
λ	is the thermal conductivity;
ν	is the kinematic viscosity;
u	is the dynamic viscosity;
D_i	is the diffusivity;
ρ	is the density (weight);
m	is the molecular weight;
$Y_i = \rho_i/\rho$	is the concentration (weight);
$c_p = \sum_i^N c_{pi} y_i$	with N denoting the number of gas components;
$Pr = \mu \bar{c}_p/\lambda$	is the Prandtl number;
$Sc_i = \mu/\rho D_i$	is the Schmidt number;
$Le_i = Pr/Sc_i$	is the Lewis number;
Q_{Ri}	is the heat of the chemical reaction per unit weight of component i;
$h_i = \int_{T_0}^{T} c_{pi} dT + \Delta_i(T_0)$	is the enthalpy of component i;
$\Delta_i(T_0)$	is the formation enthalpy of component i at temperature T_0.

Subscripts

∞	is the outer edge of a boundary layer;
p	is the plate surface;
Σ	is the material of a porous plate with a filtrating coolant;
s	is the solid matrix;
g	is the gases inside the porous plate;
e	is the porous plate at $y \to \infty$;
+	is the boundary at $y \to 0$, and $y \to -\infty$;

* is the reaction zone;
\- is the porous plate at $y \to 0$;

LITERATURE CITED

1. G. T. Sergeev, Inzh. Fiz. Zh., 23, No. 2, (1972).
2. G. T. Sergeev, Izv. Akad. Nauk BSSR, Ser. Fiz. Énerget. Nauk, No. 3, (1969).
3. G. A. Tirskii, Prikl. Matem. i Mekhan., 25, No. 2, (1961).
4. G. T. Sergeev, Inzh. Fiz. Zh., 13, No. 1, (1961).